J Therm Anal Calorim (2017) 128:1783–1792
DOI 10.1007/s10973-016-6050-1

Enhanced thermal properties of Li_2CO_3–Na_2CO_3–K_2CO_3 nanofluids with nanoalumina for heat transfer in high-temperature CSP systems

Zhaoli Zhang[1] · Yanping Yuan[1] · Liping Ouyang[1] · Qinrong Sun[1] · Xiaoling Cao[1] · Sami Alelyani[2]

Received: 21 June 2016 / Accepted: 9 December 2016 / Published online: 28 December 2016

Abstract Nanofluids of Li_2CO_3–Na_2CO_3–K_2CO_3 improved by three nano-Al_2O_3 samples are firstly prepared by means of two-step aqueous method to enhance thermal properties for high-temperature heat transfer, when used as heat transfer fluids and thermal energy systems for concentrating solar power systems. Specific heat of ternary carbonates containing Al_2O_3 of 0.2, 0.4, 0.8, 1.0, 1.4 and 2.0 mass% is measured, and nanofluids with 1.0 mass% of 20-nm Al_2O_3, 1.0 mass% of 50-nm Al_2O_3 and 0.8 mass% of 80-nm Al_2O_3 are selected as superior candidates. The maximum enhancement of specific heat is 18.5% in solid and 33.0% in liquid, 17.9% in solid and 22.7% in liquid, 13.2% in solid and 17.5% in liquid for nanofluids containing 20-, 50- and 80-nm Al_2O_3. Thermal conductivity is, respectively, improved by 23.3, 28.5 and 30.9% under the addition of Al_2O_3. New chemical bonds and crystals are scarcely formed in composites through FT-IR and XRD determination. SEM images certify that nano-Al_2O_3 are homogeneously mixed into nanofluids and this structure may be a critical incentive for enhancing thermal properties. There are no significant changes with respect to the heat flow, melting/freezing point and latent heat after the 30 circles of determination. Briefly, it can be speculated that these nanofluids will exhibit tremendous potential in the coming applications of heat transfer and thermal storage for concentrating solar power systems.

✉ Yanping Yuan
ypyuan@home.swjtu.edu.cn

[1] School of Mechanical Engineering, Southwest Jiaotong University, Chengdu 610031, Sichuan, China

[2] School for Engineering of Matter, Transport and Energy, Arizona State University, Tempe, AZ 85287, USA

Keywords Thermal properties · Nanofluids · Carbonate ternary · Heat transfer fluids · Thermal energy system

Introduction

High-temperature heat transfer fluids (HTFs) and thermal energy storage (TES) are the dominating components for effective thermal management in concentrating solar power (CSP) with the outstanding advantage of high efficiency and dispatchability, which can be incorporated into or out of power grid according to the practical requirement [1–3]. Heat transfer ability of HTFs mainly determines the thermal exchange between TES and high-temperature vapor that drives the turbine for electricity production. And the well-designed TES system that represents approximately 10–30% of the total capital cost can sustain extended thermal supply for several hours in the absence of solar radiation to reduce the radiation mismatching in time and space [4–7]. Molten salt of Li_2CO_3–Na_2CO_3–K_2CO_3 is the promising medium used in high-temperature CSP plants running with the same material for HTFs and TES due to its high melting point, excellent thermal stability and low vapor pressure [2, 8]. Unfortunately, poor thermal properties of carbonate ternary, especially small specific heat, limit the heat transfer performance which leads to be uncompetitive for CSP plants competing with traditional fossil-fueled power plants [9–11].

Nanofluids are defined as stable colloidal suspensions with the dimension of nanoparticles less than 100 nm. Referring to the literature, metallic particles and metallic oxide particles together with carbon materials are three mainly additives used in nanofluids [12–16], whereas metallic particles will be corroded in liquid molten salts that they are commonly seen in water- or organic oil-based

nanofluids [13, 17–20]. Carbon materials basically appeared with the purpose of improvement of thermal conductivity. For molten salt nanofluids, the metallic oxide particles are the preferred choice of additives in the pursuit of improved thermal properties [21–24]. It can be expected that using this enhanced eutectic as a single fluid for HTF and TES of CSP plants can dramatically reduce the cost of electricity by eliminating heat exchangers between HTF and TES for high exegetic efficiency and reducing the heat load for the freeze protection.

Extensive studies have been carried out in respect of molten salt nanofluids for the purpose of enhancing thermal properties. Myers et al. [25] prepared single salt ($NaNO_3$, KNO_3) with CuO nanoparticles in order to improve the heat transfer for thermal energy storage. Statistically significant increases in thermal conductivity were observed for KNO_3 over the entire temperature range (273–523 K), and significant increases in conductivity for $NaNO_3$ were observed only for temperatures under 423 K. Dudda and Shin [26, 27] studied $NaNO_3$–KNO_3 (60:40) with different sizes of silica nanoparticles. The enhancement of specific heat was 12.0, 19.0, 25.0 and 27.0% for 5-, 10-, 30- and 60-nm particles at 1.0% concentration by mass, respectively. Ho and Pan [28] reported effect of 50-nm alumina on the specific heat for KNO_3–$NaNO_2$–$NaNO_3$ (53:40:7 mol.%). The enhancement reached 19.9% under the optimal concentration of 0.063 mass%. Notably, there was a decrease in trend of enhanced effect as the concentration increases from 0.063 to 2.0 mass%, which might be caused by the particle agglomeration at high concentration. This molten salt in the composition of (49:30:21) was modified by the 20-nm silica in the research of Devaradjane and Shin [29]. At the concentration of 1.0 mass%, the measured values testified that the specific heat achieved approximately a 19.0% enhancement compared to the pure eutectic. Shin and Banerjee [30] evaluated the specific heat of Li_2CO_3–K_2CO_3 (62:38) in the presence of 1.0% of silica by mass with 5, 10, 30 and 60 nm of average size. Their investigations showed that an increase of about 25.0% in specific heat and the size of nanoparticles had little effect on the enhancement. SEM images of nanofluids after the melting/freezing process revealed the formation of special needle-like nanostructures, which was speculated as a potential inducement for the enhanced phenomenon. In another research of Shin and Banejee [31], Li_2CO_3–K_2CO_3 in the same composition expressed 33.0% of improvement in specific heat when mixed with alumina at the mass concentration of 1.0%. Similarly, the needle-like nanostructures were found in the study. However, other studies have scarcely reported this structure and no evidence can certify the existence of this structure in molten salt-based nanofluids. Chlorate quaternary of $BaCl_2$–NaCl–$CaCl_2$–LiCl with silica nanoparticles was prepared, and its specific heat was measured in DSC [32]. When the concentration was 1.0 mass%, the specific heat exhibited a 14.5% increase at the temperature range from 773 to 828 K.

Based on the initial pioneering efforts in this field, most available literature is related to nitrates and binary carbonate [33–35]. There is no feasible study to explore the enhancement of specific heat of Li_2CO_3–Na_2CO_3–K_2CO_3, which is regarded as the excellent medium for the next generation of high-temperature CSP plants [36]. From the above discussion, it is anticipated that specific heat of Li_2CO_3–Na_2CO_3–K_2CO_3 can be also enhanced by the similar mechanism of nanofluids. Therefore, this study aims to prepare and investigate ternary carbonate nanofluids doped with nano-Al_2O_3 (T_m = 2318.0 K, ρ = 3.960 g cm^{-3}, $C_{p,average}$ = 0.842 J g^{-1} K^{-1}). Three different sizes (20 nm, 50 nm and 80 nm) of Al_2O_3 nanoparticles picked from the reagents are chosen to research the particle size effect. Nanoparticles are firstly doped into the ternary carbonate at different concentrations by mass. Next, the measured specific heat and thermal conductivity validate the improvement of Al_2O_3 nanoparticles. Finally, the composition, structure and morphology of prepared nanofluids are characterized through FT-IR, XRD and SEM.

Materials and methods

Materials

Lithium carbonate (Li_2CO_3, content ≥99.0%), sodium carbonate (Na_2CO_3, content ≥99.8%) and potassium carbonate (K_2CO_3, content ≥99.0%) are provided by Kelong Chemical Co. as the carbonate salts. Three alumina (Al_2O_3, content ≥99.99%) in the nanoscale are bought from Aladdin chemical Co. According to the reagent instructions, their sizes are 20, 50 and 80 nm, respectively. All the chemicals are of analytical grade and used without further purification.

Preparation of nanofluids

Carbonate nanofluids in this study are prepared by two-step aqueous method, which had been proved to be an effective method to avoid the aggregation and sedimentation of nanoparticles. Three carbonates were firstly dried in a vacuum oven (DZF-6050A, Zhongxingweiye) at 393 K for 3 h to clearly remove absorbed moisture. Then, each carbonate was precisely weighed on an electronic balance (MS105DU, METTLER TOLEDO) to ensure that the mass ratio was conformed to the ternary composition (Li_2CO_3:Na_2CO_3:K_2CO_3 = 32.1:33.4:34.5 mass%). For 1.000 g of the sample, the mass is 0.321 g for Li_2CO_3, 0.334 g for Na_2CO_3 and 0.345 g for K_2CO_3. Three weighed carbonates were dissolved into 100 mL distilled water. Meanwhile, the Al_2O_3 was also added into the solution with different contents (0.2, 0.4, 0.8, 1.0, 1.4

and 2.0 mass%). The solution was under sonication for 3 h with the purpose of forming a homogeneous solution for the following process. After the ultrasonic treatment, the solution was transferred to a hot plate and heated at 473 K to completely evaporate the distilled water. Finally, the cooled mixtures in solid form were ground into powder and preserved in a glass desiccator for further utilization.

Measurement and characterization of nanofluids

Thermophysical properties, structures and morphology of improved nanofluids are investigated to explore their potentials in applications of CSP systems.

Specific heat measurement

A differential scanning calorimeter (DSC, Q20, TA) is employed to accomplish the measurement of specific heat. Each sample to be tested was sealed in a Pt crucible to prevent possible sample loss and corrosion of carbonates during measurement. The mass of samples was strictly kept within 5–10 mg. To avoid moisture absorption, each sample was firstly heated at 473 K for 5 min. In the subsequent step, the sample was heated to 873 K under the constant heating rate of 10 K min^{-1} and the sample eventually underwent an isothermal treatment for 5 min at 873 K. Three samples of each carbonate eutectic with and without Al_2O_3 were separately analyzed to confirm the reliability of the measurement and the average of specific heat were used as the results shown in this study. With indium as a standard reference material, the deviation of DSC instrument and the instrument reproducibility are ± 0.1 and $\pm 1.0\%$, separately. The value of specific heat is calculated by comparing the heat flow of samples to be tested with that of the standard sapphire provided by TA.

Thermal conductivity measurement

The thermal diffusivity and thermal conductivity of the pure eutectic and nanofluids in solid were measured using laser flash analysis instrument (LFA457, NETZSCH) at 298 K. To minimize moisture infiltration, materials were milled and kept in a drying oven prior to pressing. Next, samples were pressed into cylindrical pieces ($\Phi = 10.0$ mm) under 30.0 MPa pressure. Additionally, the sample height was about 1.0 mm to ensure the flash diffusivity effect. The measured instrument is calibrated by a graphite standard with a stated accuracy of $\pm 6.0\%$.

FT-IR characterization

In order to explore whether possible chemical reactions that occur during the formation of nanofluids may be the reason for the enhancement of thermal properties, Fourier transform infrared spectroscopy (FT-IR) is introduced to analyze the characteristic absorption peak. The structural analyses of the pure ternary and prepared nanofluids doped by Al_2O_3 were performed by using an instrument (Nicolet 6700, Thermo) with a diffuse reflectance accessory. The FT-IR spectra were recorded on a KBr pellet in the frequency range from 4000 to 400 cm^{-1}.

XRD characterization

X-ray diffraction (XRD, $\lambda = 1.7890$ Å, X'Pert Pro MPD) was used to analyze the crystal structure of samples. Numerous characteristic peaks in the diffraction spectrum could indicate the inner structure of molecules or atoms, and the composition of composite molten salts prepared in the investigation. The angle of the diffraction detected in XRD was chosen between 5° and 70°.

SEM characterization

Scanning electron microscope (SEM) mainly used secondary electron signal to observe the surface morphology of the sample. It is widely recognized as a popular technology in the determination and analysis of surface morphology in the micro- or nanoscale. Hence, the microstructure and morphology of samples were measured through the SEM performed in the instrument (Fei Inspect FEI, Netherlands). Different magnifications ($\times 1000$ and $\times 20{,}000$) of figures were acquired to compare the surface morphology and structure.

Stability

As the HTFs and TES used in CSP plants, stability is an essential element that should be considered seriously. Meanwhile, it is difficult to conduct the long-term stability testing; thus, short-term measurement of 30 circles is carried out by using the DSC instrument in order to provide available reference to the further research. The program of a circle was set as follows: samples firstly were kept isothermal for 10 min at 573 K. Then under the heating rate of 10 K min^{-1}, samples were heated to 773 K followed by another isothermal process of 10 min. After that, the temperature of samples decreased to 573 K at a cooling rate of 10 K min^{-1}. All the samples circled the above program 30 times to finish the stability determination.

With the purpose of highlighting the effect of Al_2O_3 on the stability, the melting/freezing point defined as the peak value and latent heat of samples before and after various circles (10, 20 and 30) were studied in DSC determination.

Results and discussion

Specific heat measurement

Specific heat is the dominating parameter which directly determines the heat absorption or release ability of molten salts used in CSP plants. Within the same amount of time, nanofluids improved by Al_2O_3 with larger specific heat obtain the capacity to absorb or release more thermal energy collected by heliostats/lenses when conducting heat transfer in CSP systems.

Thus, with the purpose of evaluating the specific heat of nanofluids, pure salts and three nanofluids were subjected to DSC measurement and their results are exhibited in Figs. 1–3.

Figures 1–3, respectively, show the specific heat of three nanofluids of various alumina concentration (0.2, 0.4, 0.8, 1.0, 1.4 and 2.0 mass%) in the form of solid (473–623 K) and liquid (723–873 K). Table 1 shows the value of specific heat for pure salts and three nanofluids.

As shown in Figs. 1–3 and Table 1, addition of Al_2O_3 expressed diverse enhancement of the specific heat, depending on the concentration of additives. For nanofluid of 20-nm Al_2O_3, no matter in solid and liquid, specific heat increases as the concentration increases. Solid specific heat of this nanofluid reached the maximum at the concentration of 1.0 mass%, and the value was 1.475 J g^{-1} K^{-1} which is approximately 18.5% higher than pure salts. After that, the value began to decrease when Al_2O_3 continued to increase. In liquid stage, there was an analogical change as the Al_2O_3

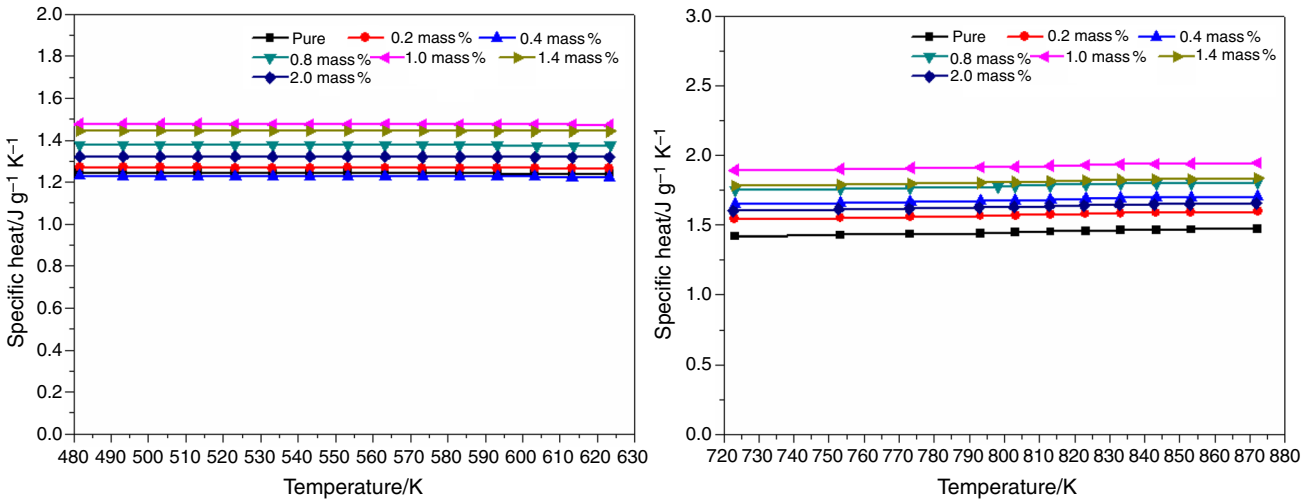

Fig. 1 Specific heat of nanofluids with 20-nm Al_2O_3

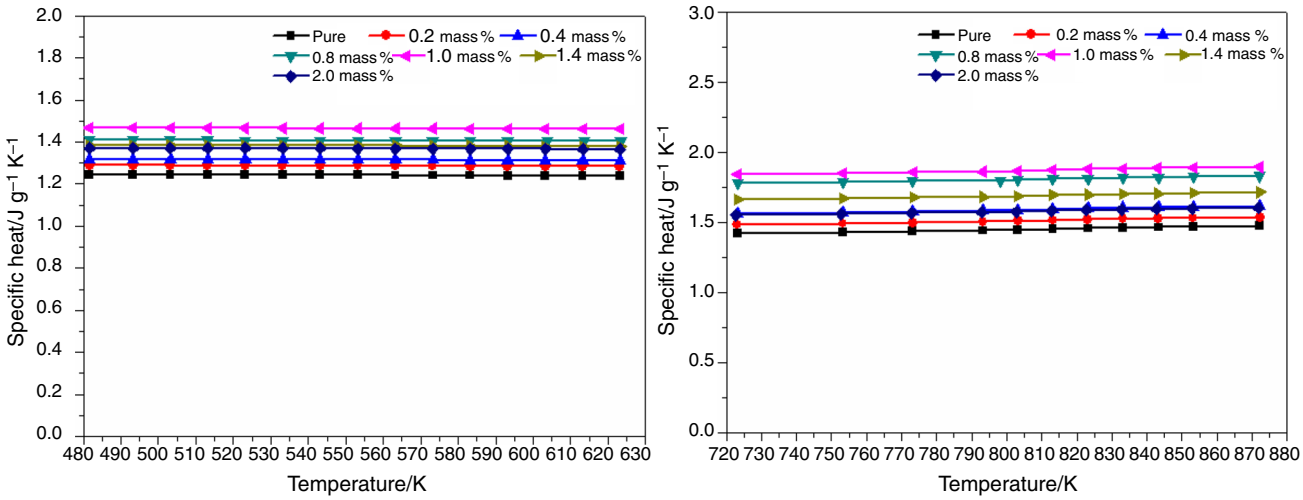

Fig. 2 Specific heat of nanofluids with 50-nm Al_2O_3

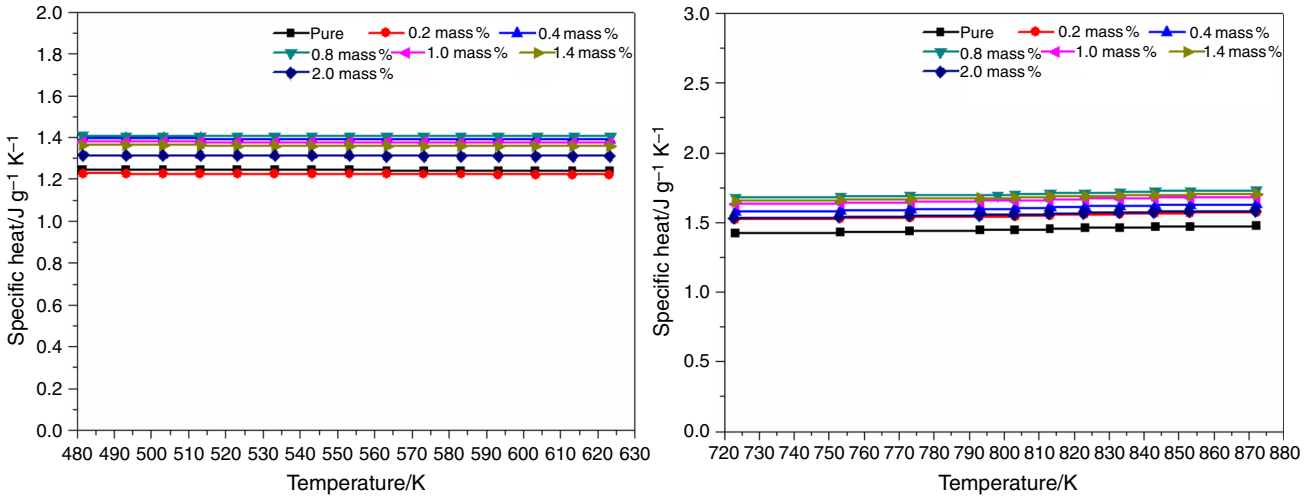

Fig. 3 Specific heat of three nanofluids with 80-nm Al_2O_3

Table 1 Specific heat of the pure salts and three nanofluids

Material	Content/mass%	$C_{p,s}$/J g^{-1} K^{-1}	Enhance/%	$C_{p,l}$/J g^{-1} K^{-1}	Enhance/%
Pure salts	–	1.243	–	1.453	–
Salts + Al_2O_3 (20 nm)	0.2	1.269	2.1	1.577	8.5
	0.4	1.337	7.6	1.685	16.0
	0.8	1.376	10.7	1.787	23.0
	1.0	1.475	18.5	1.933	33.0
	1.4	1.444	16.2	1.816	24.9
	2.0	1.321	6.3	1.713	11.8
Salts + Al_2O_3 (50 nm)	0.2	1.287	3.6	1.516	4.3
	0.4	1.315	5.9	1.596	9.6
	0.8	1.407	13.2	1.811	18.4
	1.0	1.465	17.9	1.875	22.7
	1.4	1.383	11.3	1.694	16.6
	2.0	1.369	10.2	1.583	8.9
Salts + Al_2O_3 (80 nm)	0.2	1.224	−1.7	1.551	6.8
	0.4	1.392	12.0	1.607	10.6
	0.8	1.406	13.2	1.708	17.5
	1.0	1.376	10.8	1.662	14.4
	1.4	1.361	9.5	1.683	12.1
	2.0	1.261	1.5	1.562	7.5

content increases. The specific heat of nanofluid of 20-nm Al_2O_3 climbed from 1.453 to 1.932 J g^{-1} K^{-1} with 33.0% improvement. Continuing to enlarge the content, the specific heat displayed a decline, but the enhancement was still 11.8% at 2.0 mass% of Al_2O_3.

Similarly, at 1.0 mass% Al_2O_3, the optimal specific heat was 1.465 J g^{-1} K^{-1} with 17.9% enhancement for solid nanofluids with 50-nm Al_2O_3 and 1.875 J g^{-1} K^{-1} with 22.7% enhancement for liquid nanofluids with 50-nm Al_2O_3. When it comes to nanofluids of 80-nm Al_2O_3, the enhancement of specific heat was 13.2% in solid and 17.5% in liquid at the concentration of 0.8 mass% of Al_2O_3, respectively. The largest value of specific heat for this nanofluid was 1.406 J g^{-1} K^{-1} in solid and 1.708 J g^{-1} K^{-1} in liquid. It is obvious to observe that the specific heat of nanofluids exhibits significant improvement over the original salts. Simultaneously, nanofluids with 20-nm alumina demonstrate the largest specific heat followed by nanofluids with 50-nm

alumina, and the nanofluids containing 80-nm alumina present the lowest value.

Meanwhile, the theoretical prediction from the thermal equilibrium model for molten salts mixtures presented in [32, 36] is in Eq. (1):

$$C_{p,nf} = \frac{\rho_c \times \phi_c \times C_c + \rho_p \times \phi_p \times C_{p,p}}{\rho_c \times \phi_c + \rho_p \times \phi_p} \quad (1)$$

where $C_{p,nf}$, $C_{p,c}$ and $C_{p,p}$ are effective specific heat capacity of nanofluid, carbonates and nanoparticles, respectively. ϕ_c and ϕ_p are volume fraction of carbonates and nanoparticles; ρ_c and ρ_p are density of carbonates and nanoparticles.

From the theoretical equation (Eq. (1)), specific heat of nanofluids containing nano-Al_2O_3 should be lower than that of pure salts. However, results of DSC determination show that prepared nanofluids illustrate distinctively reverse trends.

The reason for enhancement may be the special nanostructures of nano-Al_2O_3 [27]. As is well known, the smaller nanoparticles have larger specific surface area which enables them to produce more interface between particles and salts, compared to the larger nanoparticles. There also exists thermal resistance in the nanoscale interface, and more interface leads to larger thermal resistance [34]. Therefore, nanofluids with smaller nanoparticles will absorb more heat and have larger specific heat due to the existence of larger thermal resistance [37]. In addition, larger interfacial energy between the nanoparticles and molten salts may be another important reason for the enhancement of specific heat.

In the following investigation, nanofluids with 1.0 mass% of 20-nm Al_2O_3, 1.0 mass% of 50-nm Al_2O_3 and 0.8 mass% of 80-nm Al_2O_3 were selected as the candidates in the following investigation to explore the thermal properties structures and morphology.

Thermal conductivity

When used as HTFs and TES in CSP plants, thermal conductivity significantly affects the ability of thermal diffusion and the heat exchange rate. On the basic principle of the laser flash diffusivity method, the thermal conductivity of pure salts and nanofluids modified by Al_2O_3 is illustrated in Table 2.

As shown in Table 2, three samples were taken into the thermal conductivity determination and there is no larger fluctuation among three results. The maximal vibration is approximately 0.014, 0.064, 0.016 and 0.013 W m^{-1} K^{-1} for pure salts and nanofluids modified by 20-, 50- and 80-nm Al_2O_3. Thus, the laser flash analysis is a reliable method and these nanofluids exhibit extremely stable performance in thermal conductivity.

From the measured results in Table 2, it seems easy to draw the conclusion that three nanofluids upon addition of Al_2O_3 nanoparticles all display dramatic improvement to the thermal conductivity. The average thermal conductivity of nanofluid was 2.064 W m^{-1} K^{-1} for 20-nm Al_2O_3; 2.148 W m^{-1} K^{-1} for 50-nm Al_2O_3; and 2.191 W m^{-1} K^{-1} for 80-nm Al_2O_3. The enhancement caused by the addition of nanoparticles reached 23.3, 28.3 and 30.9%, respectively. Moreover, results also indicate that the enhancement of thermal conductivity for nanofluids continues to increase with the amount of the nanoparticles.

As is well known, Al_2O_3 particles uniformly scattered in the carbonate ternary is inclined to form the heat transfer network. This network can be employed as the effective path for heat transfer. Therefore, three nanofluids upon addition of Al_2O_3 nanoparticles all demonstrate statistically significant improvement over that without addition. Furthermore, smaller nanoparticles that have larger surface energy tend to agglomeration or precipitation which is averse to the formation of effective heat transfer network. The network for heat transfer will present some missing or partially incomplete structure when the agglomeration or precipitation of Al_2O_3 appears in the nanofluids. These sites will cripple the efficiency of thermal transfer, leading to the decrease trend with the addition of nanoparticles. Thus, nanofluids with 80-nm Al_2O_3 obtain the largest value of thermal conductivity.

FT-IR determination

Three prepared composite carbonate salts together with the original carbonate salts underwent the FT-IR

Table 2 Thermal conductivity of pure salts and three nanofluids

λ/W m^{-1} K^{-1}	Pure salts	Salts + Al_2O_3 (20 nm)	Salts + Al_2O_3 (50 nm)	Salts + Al_2O_3 (80 nm)
First sample	1.664	1.995	2.142	2.202
Second sample	1.670	2.079	2.138	2.178
Third sample	1.688	2.118	2.164	2.193
Average	1.674	2.064	2.148	2.191
Enhance/%	–	23.3	28.3	30.9

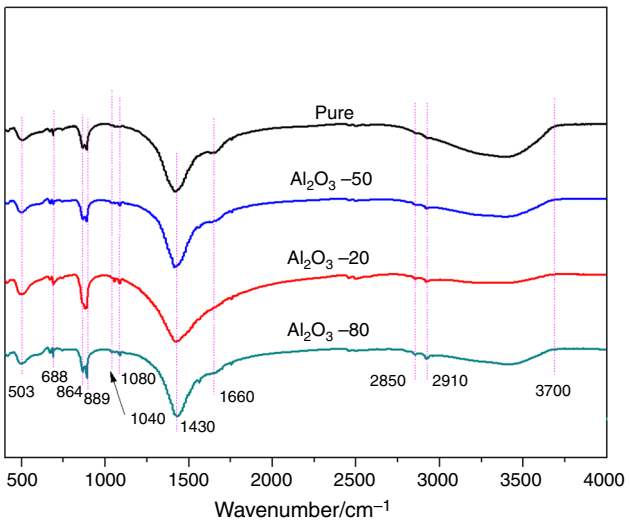

Fig. 4 FT-IR determination of the pure salts and three nanofluids

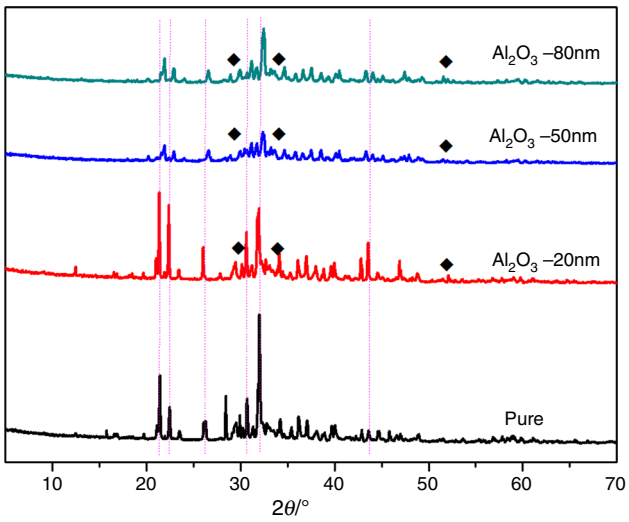

Fig. 5 XRD determination of the pure salts and three nanofluids

determination, and their characteristic absorption peaks are illustrated in Fig. 4.

As demonstrated in Fig. 4, numerous absorption peaks of corresponding compositions appeared in the four nanofluids. The locations of characteristic peaks at 2850, 2910, 1430 and 503 cm^{-1} belonged to the peculiar chemical bonds of Li_2CO_3, Na_2CO_3, K_2CO_3 and Al_2O_3. As to Li_2CO_3, Na_2CO_3 and K_2CO_3, their existence could also be verified by the absorption peaks that emerged at 688, 864, 889 and 1660 cm^{-1}.

In general, it is clear to get the conclusion that FT-IR results vary scarcely with the addition of Al_2O_3. None of the characteristic peaks for new structures are visible after modification by Al_2O_3. There are some slight shifts between FT-IR spectra of the pure ternary and the nanofluids, and this sight may be caused by a new macroscale structure formed through intermolecular forces and electrostatic interaction when the Al_2O_3 is added in the preparation. In conclusion, nanofluids can be considered as the physical mixtures without new formed materials.

XRD determination

In an effort to analyze the crystal structure after the modification of Al_2O_3 with diameters of 20, 50 and 80 nm, XRD determination was conducted in the diffraction angle from 5.0° to 70.0° and the results of carbonates before and after Al_2O_3 enhancement are represented in Fig. 5.

As illustrated in Fig. 5, various diffraction peaks were observed in these spectra. The intense diffraction peaks appearing at 29.5°, 33.7° and 51.8° were indexed to the characteristic planes of the crystal for Al_2O_3, respectively. Compared to original salts, the improved nanofluids presented unique diffraction peaks of Al_2O_3 and the results could demonstrate that additives are successfully introduced into the salts. The diffraction peaks showed the identical crystal plane distances in the three carbonate crystals. However, due to the existence of crystal doping, it is particularly observed that the locations (21.5°, 22.4°, 26.2°, 32.0° and 41.8°) of peaks in Li_2CO_3–Na_2CO_3–K_2CO_3 with Al_2O_3 nanoparticles are slightly lower than those of pure salts.

The three carbonates have a monoclinic structure and larger crystal lattice spacing. In the formation of the eutectic, three carbonates firstly form a monoclinic crystal. Then, a small amount of Al_2O_3, which possesses a different structure and smaller radius, enters into the interval of forming structure of the monoclinic crystal, leading to the occurrence of crystal doping. This doped structure is reflected in the right shift of the XRD spectra in Fig. 5.

SEM determination

In this investigation, three prepared nanofluids and original salts experienced the SEM determination and the scanned images with the magnification of ×1000 and ×20,000 are shown in Fig. 6.

From Fig. 6a, b, the original salts presented smooth surfaces and a few large particles appeared in the cross section. When nano-Al_2O_3 was added into the mixtures, the surface of the solid nanofluids became rougher than that of pure salts, as shown in Fig. 6c–h. This unsmooth structure might be produced by the inset of nano-Al_2O_3. It is also obvious that the content of roughness is becoming larger in the order of (d), (f) and (h), which is consistent with the size of the added Al_2O_3. Therefore, it can be speculated that the Al_2O_3 nanoparticles are homogeneously scattered into the mixture of nanofluids and this composition might

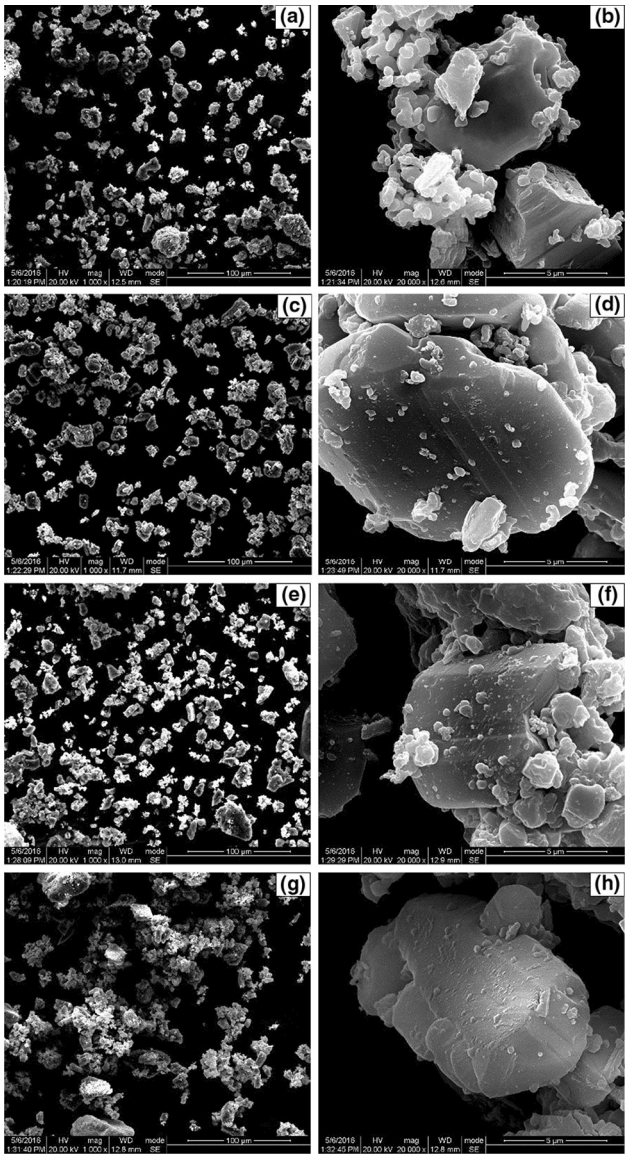

Fig. 6 Images of SEM with the magnification of ×1000 and ×20,000. **a**, **b** are the pure salts; **c**, **d** are nanofluids of 20-nm Al_2O_3; **e**, **f** are nanofluids of 50-nm Al_2O_3; **g**, **h** are nanofluids of 80-nm Al_2O_3

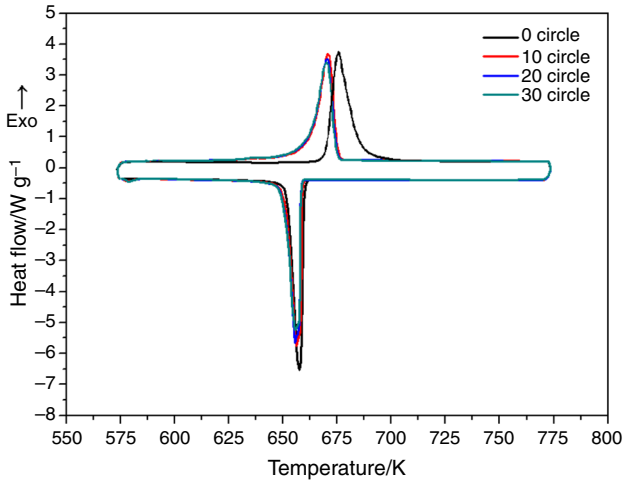

Fig. 7 DSC curves of nanofluids with 20-nm Al_2O_3 after circle determination

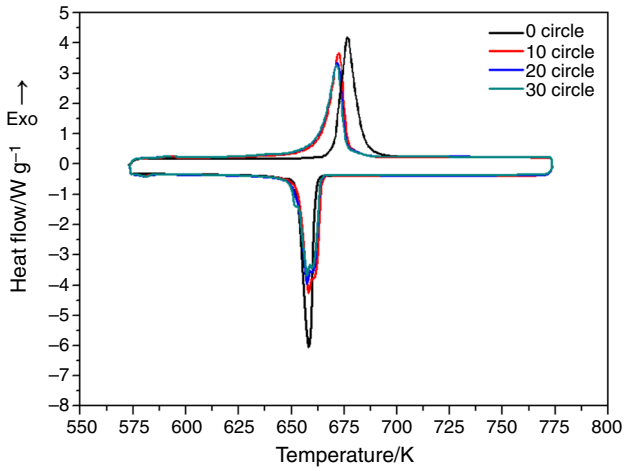

Fig. 8 DSC curves of nanofluids with 50-nm Al_2O_3 after circle determination

be the structural factor for enhancing the thermal properties.

However, the smaller nanostructure reported in [32] having a diameter of 100–150 nm and a length of up to 1–2 μm did not appear in SEM determination.

Stability

Equipped to the CSP systems, nanofluids can play an important role in the function of HTFs and TES. Hence, nanofluids with excellent stability will obtain an outstanding advantage over other materials. In this investigation, three nanofluids underwent 30 circles of stability determination. After that, these samples were subjected to DSC determination and the results are presented in Figs. 7–9 and Table 3.

As illustrated in Figs. 7–9 and Table 3, the DSC curves after 10, 20 and 30 circles presented a slight shift to the left compared to that without the circle determination. For nanofluids of 20-nm Al_2O_3, the melting point after 10, 20 and 30 circles decreased from 672.3 to 670.8, 670.9, 670.1 K, respectively. The corresponding latent heat in melting process slowly fluctuated to 222.1, 217.8 and 214.0 J g^{-1}. In the solidification of three nanofluids, freezing point presented scarcely any variation after the circle determination, whether in any one of these circles. As for the latent heat in the solidification, the value reduced to 203.3, 198.7 and 199.1 J g^{-1}, respectively.

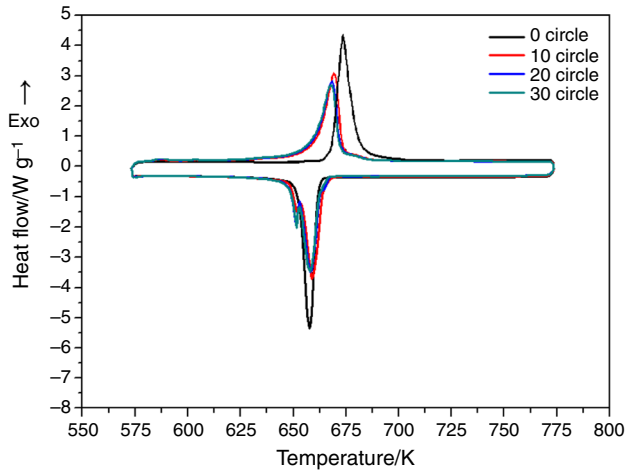

Fig. 9 DSC curves of nanofluids with 80-nm Al_2O_3 after circle determination

Table 3 Melting/freezing point and enthalpy of nanofluids before and after 30 circles

Material	Circle	T_m/K	$\Delta H_{melting}$/J g^{-1}	T_f/K	$\Delta H_{freezing}$/J g^{-1}
Pure salts	–	680.1	247.1	659.8	229.3
Salts + Al_2O_3 (20 nm)	0	672.3	230.8	659.2	210.7
	10	670.8	222.1	658.4	203.3
	20	670.9	217.8	657.8	198.7
	30	670.1	214.0	657.9	199.1
Salts + Al_2O_3 (50 nm)	0	672.3	233.1	661.0	211.8
	10	671.7	221.0	664.1	208.7
	20	671.0	219.6	663.4	204.3
	30	670.2	215.4	663.4	200.1
Salts + Al_2O_3 (80 nm)	0	671.1	239.7	661.6	208.0
	10	670.2	226.0	663.8	209.8
	20	669.5	219.1	663.1	208.6
	30	668.7	216.8	662.6	202.4

When it comes to nanofluids with 50- and 80-nm Al_2O_3, there exists the similar trend for melting/freezing point and latent heat. After 30 circles, melting point decreased to 670.2 and 668.7 K for nanofluids with 50- and 80-nm Al_2O_3. The latent heat in the melting process mildly went down to 215.4 and 216.8 J g^{-1}, respectively. During the solidification, melting point of nanofluids with 50- and 80-nm Al_2O_3 declined to 663.4 and 662.6 K and the corresponding latent heat dropped to 200.1 and 202.4 J g^{-1}, respectively.

In brief, it is apparent that there are no significant changes with respect to the heat flow, melting/freezing point and latent heat after various circles of determination. Therefore, results measured in the investigation can confirm the superior stability of these nanofluids.

Conclusions

CSP plants operated under high-temperature condition will not only generate much more electricity but also benefit the reduction of fossil fuel use and carbon emission to the environment. High-temperature nanofluids in the form of Li_2CO_3–Na_2CO_3–K_2CO_3 with Al_2O_3 nanoparticles which can be used as superior HTFs and TES are firstly prepared through two-step aqueous method with the purpose to enhance the thermal properties. Nanofluids with three different sizes of Al_2O_3 nanoparticles in various concentrations (0.2, 0.4, 0.8, 1.0, 1.4 and 2.0 mass%) underwent specific heat determination. Under the criterion of specific heat, the content of Al_2O_3 is optimized and nanofluids with 1.0 mass% of 20-nm Al_2O_3, 1.0 mass% of 50-nm Al_2O_3 and 0.8 mass% of 80-nm Al_2O_3 are selected as the superior candidates. Specific heat of nanofluids containing 20-, 50- and 80-nm alumina is improved by 18.5% in solid and 33.0% in liquid, 17.9% in solid and 22.7% in liquid, 13.2% in solid and 17.5% in liquid, respectively. The enhancement of thermal conductivity caused by the addition of Al_2O_3, respectively, reaches 23.3, 28.5 and 30.1%. By the characterization of FT-IR and XRD, three improved nanofluids are proved to be the physical mixtures and there are no new chemical bonds formed in them. It can be speculated from the SEM images that the Al_2O_3 nanoparticles are homogeneously scattered into the mixtures of nanofluids and this special structure might be an important factor for enhancing the thermal properties. Finally, there are no significant changes in heat flow, melting/freezing point and latent heat between the original nanofluids and those after the stability determination.

In conclusion, results from determination can confirm the superior stability of nanofluids and it can be anticipated that they will exhibit tremendous potential in the coming application of HTFs and TES for CSP systems.

Acknowledgements This work was supported by Sichuan Province Youth Science and Technology Innovation Team of Building Environment and Energy Efficiency (2015TD0015) and 2015 Cultivation Program for the Excellent Doctoral Dissertation of Southwest Jiaotong University.

References

1. Liu M, Steven Tay NH, Bell S, Belusko M, Jacob R, Will G, et al. Review on concentrating solar power plants and new developments in high temperature thermal energy storage technologies. Renew Sustain Energy Rev. 2016;53:1411–32.
2. Xu B, Li P, Chan C. Application of phase change materials for thermal energy storage in concentrated solar thermal power plants: a review to recent developments. Appl Energy. 2015;160:286–307.

3. Ahammed N, Asirvatham LG, Wongwises S. Effect of volume concentration and temperature on viscosity and surface tension of graphene–water nanofluid for heat transfer applications. J Therm Anal Calorim. 2016;123(2):1399–409.
4. Li G. Sensible heat thermal storage energy and exergy performance evaluations. Renew Sustain Energy Rev. 2016;53:897–923.
5. Veluswamy HP, Wong AJH, Babu P, Kumar R, Kulprathipanja S, Rangsunvigit P, et al. Rapid methane hydrate formation to develop a cost effective large scale energy storage system. Chem Eng J. 2016;290:161–73.
6. Bellan S, Alam TE, González-Aguilar J, Romero M, Rahman MM, Goswami DY, et al. Numerical and experimental studies on heat transfer characteristics of thermal energy storage system packed with molten salt PCM capsules. Appl Therm Eng. 2015;90:970–9.
7. Vignarooban K, Xu X, Arvay A, Hsu K, Kannan AM. Heat transfer fluids for concentrating solar power systems—a review. Appl Energy. 2015;146:383–96.
8. Zhao CY, Wu ZG. Thermal property characterization of a low melting-temperature ternary nitrate salt mixture for thermal energy storage systems. Sol Energy Mater Sol Cells. 2011;95(12):3341–6.
9. Mirmasoumi S, Behzadmehr A. Effect of nanoparticles mean diameter on mixed convection heat transfer of a nanofluid in a horizontal tube. Int J Heat Fluid Flow. 2008;29(2):557–66.
10. Wen D, Ding Y. Experimental investigation into convective heat transfer of nanofluids at the entrance region under laminar flow conditions. Int J Heat Mass Transf. 2004;47(24):5181–8.
11. Beheshti A, Shanbedi M, Heris SZ. Heat transfer and rheological properties of transformer oil-oxidized MWCNT nanofluid. J Therm Anal Calorim. 2014;118(3):1451–60.
12. Tao YB, Lin CH, He YL. Preparation and thermal properties characterization of carbonate salt/carbon nanomaterial composite phase change material. Energy Convers Manag. 2015;97:103–10.
13. Heris SZ, Esfahany MN, Etemad SG. Experimental investigation of convective heat transfer of Al_2O_3/water nanofluid in circular tube. Int J Heat Fluid Flow. 2007;28(2):203–10.
14. Heris SZ, Etemad SG, Esfahany MN. Experimental investigation of oxide nanofluids laminar flow convective heat transfer. Int Commun Heat Mass. 2006;33(4):529–35.
15. Akbari M, Behzadmehr A, Shahraki F. Fully developed mixed convection in horizontal and inclined tubes with uniform heat flux using nanofluid. Int J Heat Fluid Flow. 2008;29(2):545–56.
16. Maïga SEB, Palm SJ, Nguyen CT, Roy G, Galanis N. Heat transfer enhancement by using nanofluids in forced convection flows. Int J Heat Fluid Flow. 2005;26(4):530–46.
17. Moghaddam MB, Goharshadi EK, Entezari MH, Nancarrow P. Preparation, characterization, and rheological properties of graphene–glycerol nanofluids. Chem Eng J. 2013;231:365–72.
18. Xu Y, Zheng Q, Song Y. Comparison studies of rheological and thermal behaviors of ionic liquids and nanoparticle ionic liquids. Phys Chem Chem Phys. 2015;17(30):19815–9.
19. Toghraie D, Chaharsoghi VA, Afrand M. Measurement of thermal conductivity of ZnO–TiO_2/EG hybrid nanofluid. J Therm Anal Calorim. 2016;125(1):527–35.
20. Esfe MH, Saedodin S. Turbulent forced convection heat transfer and thermophysical properties of MgO-water nanofluid with consideration of different nanoparticles diameter, an empirical study. J Therm Anal Calorim. 2015;119(2):1205–13.
21. Habibzadeh S, Kazemi-Beydokhti A, Khodadadi AA, Mortazavi Y, Omanovic S, Shariat-Niassar M. Stability and thermal conductivity of nanofluids of tin dioxide synthesized via microwave-induced combustion route. Chem Eng J. 2010;156(2):471–8.
22. Mirmasoumi S, Behzadmehr A. Numerical study of laminar mixed convection of a nanofluid in a horizontal tube using two-phase mixture model. Appl Therm Eng. 2008;28(7):717–27.
23. Zhang ZL, Yuan YP, Zhang HQ, Cao XL, Sun LL, Phelan PE. Thermal properties of ternary carbonate/T-ZnOw for heat transfer in high-temperature concentrating solar power systems. Compos Part A. 2016. doi:10.1016/j.compositesa.2016.11.026.
24. Timofeeva EV, Routbort JL, Singh D. Particle shape effects on thermophysical properties of alumina nanofluids. J Appl Phys. 2009;106(1):014304.
25. Myers PD, Alam TE, Kamal R, Goswami DY, Stefanakos E. Nitrate salts doped with CuO nanoparticles for thermal energy storage with improved heat transfer. Appl Energy. 2016;165:225–33.
26. Dudda B, Shin D. Effect of nanoparticle dispersion on specific heat capacity of a binary nitrate salt eutectic for concentrated solar power applications. Int J Therm Sci. 2013;69:37–42.
27. Shin D, Banerjee D. Enhanced specific heat capacity of nanomaterials synthesized by dispersing silica nanoparticles in eutectic mixtures. J Heat Transf. 2013;135(3):032801.
28. Ho MX, Pan C. Optimal concentration of alumina nanoparticles in molten Hitec salt to maximize its specific heat capacity. Int J Heat Mass Transf. 2014;70:174–84.
29. Bahiraei Mehdi. A numerical study of heat transfer characteristics of CuO–water nanofluid by Euler–Lagrange approach. J Therm Anal Calorim. 2016;123(2):1591–9.
30. Shin D, Banerjee D. Enhanced specific heat of silica nanofluid. J Heat Transf. 2011;133(2):024501.
31. Shin D, Banerjee D. Enhanced thermal properties of SiO_2 nanocomposite for solar thermal energy storage applications. Int J Heat Mass Transf. 2015;84:898–902.
32. Shin D, Banerjee D. Enhancement of specific heat capacity of high-temperature silica-nanofluids synthesized in alkali chloride salt eutectics for solar thermal-energy storage applications. Int J Heat Mass Transf. 2011;54(5–6):1064–70.
33. Chieruzzi M, Miliozzi A, Crescenzi T, Kenny JM. A new phase change material based on potassium nitrate with silica and alumina nanoparticles for thermal energy storage. Nanoscale Res Lett. 2015;10:273.
34. Chieruzzi M, Cerritelli GF, Miliozzi A, Kenny JM. Effect of nanoparticles on heat capacity of nanofluids based on molten salts as PCM for thermal energy storage. Nanoscale Res Lett. 2013;8:448.
35. Fernández AG, Ushak S, Galleguillos H, Pérez FJ. Development of new molten salts with $LiNO_3$ and $Ca(NO_3)_2$ for energy storage in CSP plants. Appl Energy. 2014;119:131–40.
36. Shin D, Tiznobaik H, Banerjee D. Specific heat mechanism of molten salt nanofluids. Appl Phys Lett. 2014;104(12):121914.
37. Shenogin S. Role of thermal boundary resistance on the heat flow in carbon-nanotube composites. J Appl Phys. 2004;95(12):8136.